

# MODELING STUDIES FOR SYNCHROTRON-RADIATION-INDUCED ELECTRON PRODUCTION IN THE VACUUM CHAMBER WALLS AT CESR TA

S. Poprocki, J.A. Crittenden, D.L. Rubin and D. Sagan  
CLASSE, Cornell University, Ithaca NY 14853

## Abstract

We report on calculations of electron production by synchrotron radiation absorbed in the vacuum chamber walls of the Cornell Electron Storage Ring (CESR). These electrons are the source of electron clouds which limit the performance of storage rings by causing betatron tune shifts, instabilities and emittance growth. Until now, cloud buildup modeling codes have used ad hoc models of the production of the seed electrons. We have employed the photon scattering code Synrad3D to quantify the pattern of absorbed photons around the CESR ring, including the transverse distribution on the wall of the beam-pipe. These distributions in absorbed photon energy and incident angle are used as input to Geant4-based simulations of electron emission from the walls. The average quantum efficiency is found to vary dramatically with the location of the absorption site, owing to the distribution in impact energies and angles. The electron production energy spectrum plays an important role in the modeling of electron cloud buildup, where the interplay of production energy and acceleration by the beam bunches determines the time structure and multipacting characteristics of the cloud.

## INTRODUCTION

The buildup of high densities of low-energy electrons has been recognized as an important operational limitation in a variety of accelerator facilities since the 1960s [1]. In positron storage rings such as KEKB and the Cornell Electron Storage Ring (CESR), as well as in the proton rings at the Large Hadron Collider, a primary source of electron production is synchrotron-radiation-induced photo-effect processes in the vacuum chamber walls. Thus the incident photon rate and quantum efficiency for producing electrons are critical factors in the time dependence of the electron densities and their interaction with the beam bunches. The quantum efficiency depends strongly on the wall material and surface properties, and on the incident photon energy and angle distributions. These determine the longitudinal and azimuthal electron production locations, including the magnetic field environments on which the subsequent evolution of the cloud depends. In addition, the cloud dynamics depend crucially on the photo-produced electron energy distribution, since, together with the momentum kicks imparted by the beam bunches, they determine the cloud density profile present at the arrival time of succeeding bunches.

Joining a multi-decade collaborative effort, the CESR Test Accelerator project [2] has undertaken a series of measurements, both local and ring-wide, to quantify, characterize

and model the buildup of electron clouds, with the goal of extending the predictive power of the models to include betatron tune shifts and emittance growth and contributing to the robust design of future accelerator facilities. Recent experimental and modeling work on tune shifts increasing along a train of positron bunches has made obvious the necessity of the present study of photo-electron production in the CESR vacuum chamber walls throughout the entire circumference of the ring.

## SYNCHROTRON RADIATION PHOTON TRACKING CALCULATION

An essential tool in this study is the photon-tracking calculation Synrad3D [3]. It provides for the generation of individual photons and incorporates a user-defined detailed model of the vacuum chamber to model the reflection and absorption of photons using the Bmad library [4] and X-ray data from and LBNL database [5]. Figure 1 shows a plan view of photon trajectories in a region of the CESR ring which includes X-ray beamline exit windows, where incident photons are not included in the tally of electron-producing photon strikes.

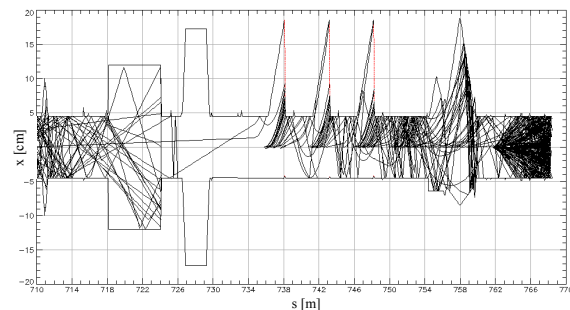


Figure 1: Top down view ( $x$  vs.  $s$ ) for a portion of the CESR ring, showing photon tracks (black lines). The red vertical lines represent X-ray beam line exit ports, and any photon hitting those surfaces are terminated and not included in the absorbed photon-rate.

Photon reflectivity plays a crucial role in electron cloud buildup, since it determines the azimuthal distribution of photon absorption sites around the ring. Absent photon reflectivity, very few photons could be absorbed on the top and bottom of the beampipe, where photoelectron production is the primary source of cloud production in the vertical plane containing the beam. Figure 2 shows the fraction of photons reflected as a function of photon energy for a 5-degree grazing and for aluminum with C or CO surface

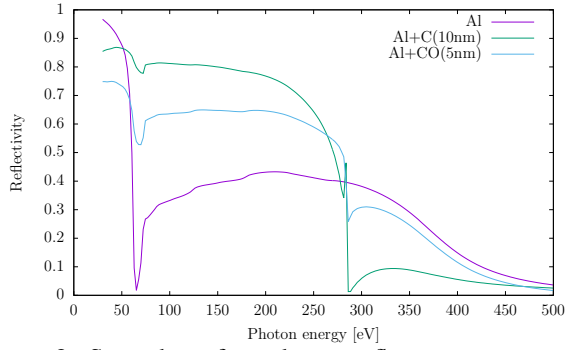


Figure 2: Smooth-surface photon reflectivity versus photon energy for aluminum, aluminum with a 10 nm carbon layer, and aluminum with a 5 nm carbon monoxide layer, for photons incident at a 5 degree grazing angle. Data from [5].

layers. In validating our modeling studies, we have found it advantageous to use the 5 nm CO layer.

These photon tracking calculations provide our simulations with a sample of  $10^6$  absorbed photon sites, including incident energy and angle. Figure 3 shows the azimuthal distribution of the average number of prior reflections for absorbed photons. The strong energy dependence of the reflectivity results in a strong variation of absorbed photon energy with azimuth, with important consequences for the quantum efficiency and electron production energies arising from the atomic shell properties of the wall material. The average energy of the absorbed photons in the azimuthal ranges  $|\Phi_{180}| < 1.5^\circ$ ,  $1.5^\circ < |\Phi_{180}| < 1.5^\circ$  and  $|\Phi_{180}| > 165^\circ$  is 3078 eV, 172 eV and 340 eV, respectively.

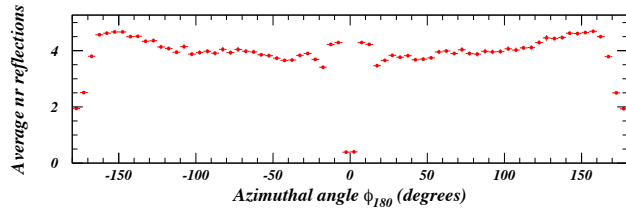


Figure 3: Average number of photon reflections as function of the azimuthal angle  $\Phi_{180}$  of the photon absorption site, where  $\Phi_{180}$  ranges from  $-180$  to  $+180$  degrees with its origin in the mid-plane on the outside of the ring. For  $|\Phi_{180}| < 1.5$  degrees, 83% of the photons are unreflected.

## GEANT4

Significant progress in simulating low-energy electromagnetic processes has been achieved over the past decade in the Geant4 simulations toolkit [6, 7], including both photoelectron production and atomic de-excitation processes in a wide variety of materials [8]. We employ this modeling tool to determine quantum efficiency values and electron momentum distributions in each of 720 azimuthal bins for field-free and dipole regions separately, generating a total of  $1.5 \times 10^8$  events. Examples of such events are shown in Fig. 4. We thus obtain a value for the electron production rate specific to the photon incident angle and energy distribution in each

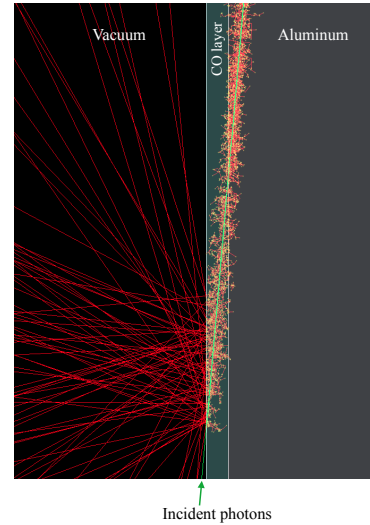


Figure 4: Tracks from incident 300 eV photons (green) and subsequently generated electrons (red) from Geant4. The outgoing angular distribution of electrons is normal to the surface on average.

azimuthal bin, including (relatively rare) multi-electron production events. Figure 5 shows the detail with which Geant4 calculates average electron production rate for various wall materials. In addition, we obtain distributions of electron

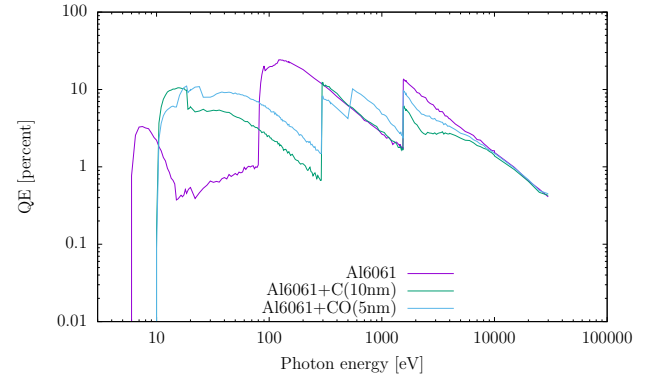


Figure 5: Quantum efficiency versus photon energy for photons incident at a 5-degree grazing angle, for aluminum, aluminum with carbon layer, and aluminum with carbon monoxide layer. QE jumps for photon energies above various atomic shell transition energies: Aluminum  $L_{II}$  and  $L_{III}$  (73 eV), Carbon K (284 eV), Oxygen K (543 eV), and Aluminum K (1560 eV).

production energy and angle as a function of azimuthal production location for any chosen region of the CESR ring (see Fig. 6). Our modeling has shown that it is important and, to acceptable accuracy, sufficient to differentiate between the field-free and dipole-occupied regions, comprising 17% and 66% of the ring, respectively. Figures 7 and 8 show azimuthal distributions in average photon absorption rate and quantum efficiency obtained for our recent modeling work [9]. The electron production energy distribution is of particular importance, since the dependence of, for example, betatron tune shifts varies dramatically, with beam bunch

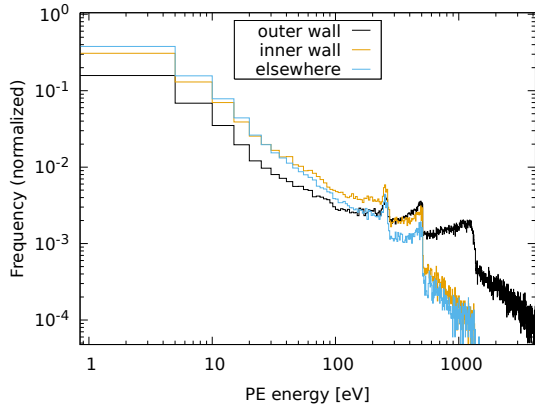


Figure 6: Photoelectron energy distributions for photoelectrons on the outside wall, inside wall, and everywhere else along the vacuum chamber in dipoles. Since lower energy photons are more likely to be reflected from the outer wall, the inner wall and elsewhere (including top & bottom) have more lower energy photoelectrons. Distributions are normalized to unit area and input to electron cloud build-up simulations [9].

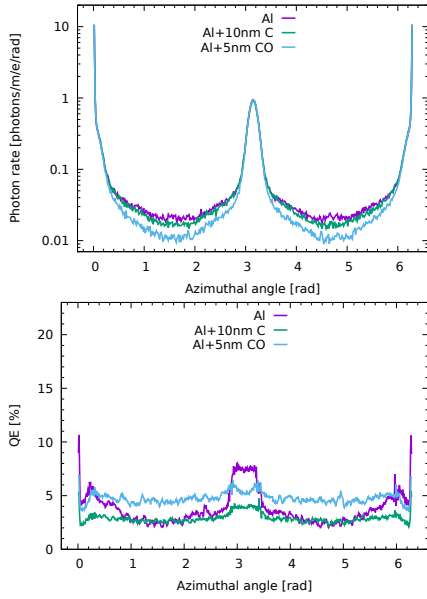


Figure 7: Azimuthal dependence of photon absorption rate (top) and quantum efficiency (bottom) for field-free regions for aluminum and aluminum with a carbon or carbon monoxide layer.

population between  $3 \times 10^{10}$  and  $9 \times 10^{10}$  positrons/bunch, and the associated beam kicks for electrons produced at the wall are comparable to the electron production energies. These Geant4 simulations show that the primary sources of high-energy electrons ( $> 100$  eV) are atomic de-excitation processes, such as the Auger effect. The contribution of such electrons to cloud development is greater at lower bunch population, since their kinetic energies provide for higher subsequent secondary yields, replacing the effect of strong momentum kicks from the beam bunches. The simulation results for the photoelectron energy distributions show sub-

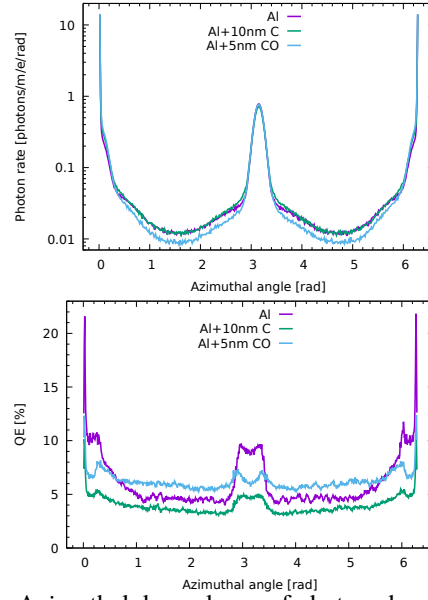


Figure 8: Azimuthal dependence of photon absorption rate (top) and quantum efficiency (bottom) for dipole-occupied regions for aluminum and aluminum with a carbon or carbon monoxide layer.

stantial high-energy tails, resulting in an average energy in the photon absorption site azimuthal ranges  $|\Phi_{180}| < 1.5^\circ$ ,  $1.5^\circ < |\Phi_{180}| < 165^\circ$  and  $|\Phi_{180}| > 165^\circ$  is 2134 eV, 152 eV and 258 eV, respectively. These energy distributions, as well as the average quantum efficiency values, are provided in 0.5 degree azimuthal bins independently for field-free and dipole regions of the CESR ring as input to the electron cloud buildup calculations described in [9].

## SUMMARY

Motivated by the need for a detailed model for the production of electrons by synchrotron-radiation photons to model CESR-TA measurements of betatron tune shifts and emittance growth in bunched positron beams, we have implemented a Geant4-based post-processor for the Synrad3D photon-tracking code. We find that the quantum efficiency and electron production kinematics depend strongly on the vacuum chamber wall characteristics as well as the location of photon absorption sites around the ring and the incident photon grazing angles and energies. This study can provide important input to electron cloud buildup modeling codes used at a wide variety of accelerators for purposes of understanding phenomena including betatron tune shifts, emittance growth, RF phase shifts, various types of instabilities and heat loads.

## ACKNOWLEDGMENTS

The authors wish to acknowledge important contributions from the technical staffs of the Wilson Laboratory. This work is supported by National Science Foundation and by the US Department of Energy under contract numbers PHY-0734867, PHY-1002467 and DE-FC02-08ER41538 and DE-SC0006505.

## REFERENCES

- [1] F. Zimmermann, “Electron-Cloud Effects in Past & Future Machines—Walk through 50 Years of Electron-Cloud Studies,” in *Proceedings of ECLOUD 2012: Joint INFN-CERN-EuCARD-AccNet Workshop on Electron-Cloud Effects, La Biodola, Elba, Italy*, R. Cimino, G. Rumolo & F. Zimmermann, Eds., CERN, Geneva, Switzerland (2013), CERN-2013-002, p. 9–17.
- [2] “The CESR Test Accelerator Electron Cloud Research Program: Phase I Report,” Tech. Rep. CLNS-12-2084, LEPP, Cornell University, Ithaca, NY (Jan. 2013).
- [3] G. Dugan & D. Sagan, “SYNRAD3D Photon Propagation and Scattering Simulations,” in *Proceedings of ECLOUD 2012: Joint INFN-CERN-EuCARD-AccNet Workshop on Electron-Cloud Effects, La Biodola, Elba, Italy*, R. Cimino, G. Rumolo & F. Zimmermann, Eds., CERN, Geneva, Switzerland (2013), CERN-2013-002, p. 117–129.
- [4] D. Sagan, “Bmad: A Relativistic Charged Particle Simulation Library,” *Nucl. Instrum. Methods Phys. Res.* **A558**, p. 356–359 (Mar. 2006).
- [5] B. L. Henke, E. M. Gullikson & J. C. Davis, “X-Ray Interactions: Photoabsorption, Scattering, Transmission, and Reflection at  $E = 50\text{--}30,000$  eV,  $Z = 1\text{--}92$ ,” *At. Data Nucl. Data Tables* **54**, p. 181–342 (Jul. 1993).
- [6] S. Agostinelli *et al.*, “Geant4—a simulation toolkit,” *Nuclear Instruments and Methods in Physics Research Section A: Accelerators, Spectrometers, Detectors and Associated Equipment* **506**, p. 250 – 303 (2003).
- [7] J. Allison *et al.*, “Recent developments in Geant4,” *Nuclear Instruments and Methods in Physics Research Section A: Accelerators, Spectrometers, Detectors and Associated Equipment* **835**, p. 186 – 225 (2016).
- [8] S. Incerti *et al.*, “Simulation of Auger electron emission from nanometer-size gold targets using the Geant4 Monte Carlo simulation toolkit,” *Nuclear Instruments and Methods in Physics Research Section B: Beam Interactions with Materials and Atoms* **372**, p. 91 – 101 (2016).
- [9] S. Poprocki *et al.*, “Progress in measurement and modeling of electron cloud effects at CESR-TA,” in *IPAC2018: Proceedings of the 9th International Particle Accelerator Conference, Vancouver, BC, Canada* (2018), Paper THPAF025.